MTAP deficiency reshapes the intratumoral immune landscape

By

Ssu-Wei Hsu

THESIS

Submitted in partial satisfaction of the requirements for the degree of

MASTER OF SCIENCE

in

INTEGRATIVE PATHOBIOLOGY

in the

School of Veterinary Medicine

of the

UNIVERSITY OF CALIFORNIA

DAVIS

Approved:

_____

Reen Wu, Chair

_____

Su Hao Lo

_____

Weici Zhang

Committee in Charge

2021

MTAP deficiency reshapes the intratumoral immune landscape

Ssu-Wei Hsu

ABSTRACT

Methylthioadenosine phosphorylase (MTAP) is an enzyme involved in the polyamine biosynthesis pathway, catalyzing the phosphorylation of methylthioadenosine (MTA) for the regeneration of methionine and adenine. Notably, MTAP has been found frequently deleted in many cancers, which was associated with worse prognosis. This study demonstrated MTAP regulated tumor-intrinsic immune-related pathways including PI3K/AKT, MEK/ERK, and JAK/STAT. MTAP-deficient tumor cells exerted immunosuppression and evasion by elevating pro-tumoral cytokines, programmed death-ligand 1 (PD-L1) and the tolerance of immune cell-mediated killing. The results from humanize mice indicated that MTAP-deficiency mediated immune dysfunction and attenuated immune responses. Furthermore, from CyTOF analysis, MTAP deficiency reshaped immune cell responses to tumor cells and impaired intratumoral immunity to support tumorigenesis *in vitro* and *in vivo*. These results indicate that MTAP deletion reconstructs the tumor microenvironment via cytokine reprogramming and restructuring of immune infiltrates thereby promoting cancer malignancy.

INTRODUCTION

Advancements in the field of oncoimmunology have revolutionized the progression of cancer research, especially in delineating tumor heterogeneity and developing innovative treatments. Immune checkpoint inhibitors (ICIs) targeting PD-1/PD-L1 axis have demonstrated successful applications across a broad range of advanced cancer types such as lung cancer, melanoma, and renal cell carcinoma (RCC)[1-4], and compared to traditional therapies, ICIs prove to potentiate more long-lasting effects[4]. These monoclonal antibody-based therapies recuperate T-cell activity by dampening co-inhibitory signaling from the aforementioned axis, thus strengthening antitumor immunity[5]. Despite the pronounced advantages of ICIs, there are still many challenges that impede effective treatment and management. In addition to immune-related adverse events, the objective response rates (ORR) for PD-1/PD-L1 inhibitors only fare around 20%-30%[6 7]. Although PD-L1 expression levels within tumors is employed as an indicative marker for ICI treatment, PD-L1 expression was found weakly correlated with response rate to PD-1/PD-L1 inhibitors[8 9], suggesting the insufficiency of identification methods that indicate which patients will benefit from such therapies.

Other potential mechanisms responsible for the low ORR to PD-1/PD-L1 inhibitors may

be attributed to the complicated tumor microenvironment, particularly the immune cells[10]. "Hot" tumors are characterized by high T cell density and IFN-γ level, and this phenotype has been leveraged as a favorable biomarker to predict patient response to ICIs. In contrast, "cold" tumors contain low proportions of immune infiltrates, impairing effective elimination of malignant cells. Such tumors also include higher densities of tumor-associated macrophages (TAMs), myeloid-derived suppressor cells (MDSCs), or regulatory T cells (Tregs), higher secretion of anti-inflammatory cytokines e.g. IL-10 and VEGF, and exhibit poor clinical outcomes[11]. Ultimately, the absence of immune responses and the presence of immunosuppressive cells concomitant with cytokine reprogramming establishes a drastically immunosuppressive cellular landscape that promotes unresponsiveness to immunotherapy[12]. Therefore, in order to overcome the challenges of ICIs, there is an urgent need to find biomarkers that direct the efficacy of ICIs and new means aside from PD-L1 staining to predict which patient population will respond.

Methylthioadenosine phosphorylase (MTAP) is an enzyme involved in the polyamine biosynthesis pathway, catalyzing the phosphorylation of methylthioadenosine (MTA) for the regeneration of methionine and adenine[13]. In addition to functioning in metabolism, MTAP also regulates protein arginine dimethylation by which MTA inhibits the catalytic

activity of PRMT5[14-16]. Notably, MTAP has been found frequently deleted in many cancers[13 14]. In both lung cancer and RCC patients, MTAP loss was associated with worse prognosis partly by upregulating IGF1R activity and vimentin abundance to aggravate tumor progression and malignancy[17]. Intratumoral MTA levels were also shown more abundant compared to matched non-malignant tissues[18], and higher *in vitro* MTA level suppressed T cell proliferation and effector function, NK cell cytotoxicity and MHC II transactivation[19-21], indicating that the consequences of MTAP loss sustain significant effects on surrounding immune cells. Given burgeoning evidence toward the ever-expanding role of MTAP in the tumor microenvironment, it is imperative to address key issues concerning MTAP-mediated tumor immunity.

Here we screened the transcriptome of MTAP-manipulated tumor cells to examine tumor-intrinsic immune-related pathways. Following these screenings, we further inoculated tumor cells into humanized immunocompetent mice and conducted mass cytometry (CyTOF) analysis to evaluate whether MTAP deficiency remodels immune profiles and contributes to immune evasion. The aim of this study is to identify novel molecular mechanisms that can bridge knowledge gaps in oncoimmunology, paving the way for future therapies and clinical translations.

RESULTS

MTAP deficiency alters tumor-intrinsic immune-related pathways

To comprehensively explore the effect of MTAP deficiency on cellular processes, RNA-sequencing was conducted in CL1-5 Mock control (Mock) and MTAP-overexpressing (MTAP) cells or CL1-0 and 786-0 MTAP-intact (WT) and MTAP-knockout (KO) cells followed by Gene Set Enrichment Analysis. Among the top 20 hallmark gene sets (Figure 1A), several were related to immune signaling: TNFA_SIGNALING_VIA_NFKB, INFLAMMATORY_RESPONSE, IL6_JAK_STAT3_SIGNALING, INTERFERON_GAMMA_RESPONSE, INTERFERON_ALPHA_RESPONSE, IL2_STAT5_SIGNALING (Figure 2). Pathway enrichment analysis of differentially expressed genes from CL1-0 WT/KO cells also showed that CXCR4, IL-5 and IFN-γ signalings were significantly enriched (Figure 1B). Proteomic alteration of cells in response to MTAP knockout was analyzed by reverse phase protein array and the results of pathway and network analysis demonstrated signalings of immune response (Figure 1C) via PI3K/AKT, MEK/ERK, and JAK/STAT pathways (Figure 1D). These results encouraged us to investigate the ramifications of MTAP deficiency in tumor immunity.

MTAP-deficient tumor cells exert immunosuppression and evasion

The altered intrinsic immune signalings in MTAP-deficient tumor cells indicate a potential alteration of cytokine secretome. Luminex assays were utilized to measure the basal level of cytokines secreted by MTAP WT/KO cancer cells. Cytokines with anti-tumoral properties including GM-CSF, IL-1α, IL-1β, IL-12 and IFN-γ were more abundant from MTAP WT cells, while RANTES, HGF, VEGF, IL-6, IL-8 and IL-9 considered as pro-tumoral cytokines were more plentiful in the supernatant of MTAP KO cells (Figure 3A), suggesting an immunosuppressive effect originated from MTAP deficiency. In addition to cytokine reprogramming, tumor cells undergo immune escape also by upregulating the expression of immune checkpoint inhibitory ligands e.g. programmed death-ligand 1 (PD-L1). We thus sought to determine the protein level of PD-L1 by Western blot (Figure 3B) and immunofluorescence (Figure 3C), and found that PD-L1 protein is elevated upon MTAP knockout. Moreover, the cell surface abundance of PD-L1 is more in MTAP KO cells than in WT cells (Figure 3D). To better reflect the real cytotoxic abilities, PBMCs were unstimulated and co-cultured with MTAP WT/KO tumor cells. Results from flow cytometric analysis showed that MTAP knockout rendered tumor cells tolerant of immune cell-mediated killing (Figure 3E), confirming the regulatory role of MTAP deficiency in immunosuppression.

MTAP deficiency leads to immune dysfunction and attenuated immune responses

The observed immunomodulatory effects of tumor cells with MTAP loss *in vitro* prompted us to evaluate the tumorigenesis and tumor immunity in humanized mouse xenograft models. First, immunodeficient NSG-SGM3 mice were inoculated with MTAP WT/KO or Mock/MTAP-overexpressing tumor cells, and the results are consistent to our previous findings that MTAP deficiency promotes tumorigenesis (Figure 4A). Surprisingly, when tumor cells were inoculated into the NSG-SGM3 mice engrafted with human hematopoietic stem cells, the difference of tumor size between WT/KO or Mock/MTAP groups became more overwhelming (Figure 4B). This discrepancy suggested that MTAP deficiency may either block immune activation or promote immune dysfunction and hijack the immune system. To further investigate the underlying molecular signalings regulating immune response mediated by MTAP WT or KO cells, CL1-0 cells co-cultured with unstimulated PBMCs or not were subjected to RNA-sequencing, and the differentially expressed genes in only WT cells or in only KO cells were analyzed for enriched pathways respectively (Figure 4C). The top-ranked pathways of WT cells co-cultured with PBMCs (WT+PBMC) were centered on IL-12 signalings, exhibiting anti-tumoral immunity, while MTAP KO cells switched to lung cancer progression signaling in response to PBMCs exposure (Figure 4D). The following GSEA analysis also

demonstrated that compared to WT cells, MTAP KO cells showed weaker responses to IL-12 downstream IFN-γ (Figure 4E), supporting the observations in NSG-SGM3 mice that MTAP-deficient tumors escape immune surveillance and progress.

MTAP deficiency reshapes immune cell responses to tumor cells

We next performed Luminex assays to ascertain whether cytokine secretion patterns were altered corresponding to the phenotypes observed in NSG-SGM3 mice after MTAP WT/KO tumor cells were co-cultured with PBMCs. Compared to the secretion patterns of tumor cells only (Figure 3A), almost all cytokine levels were evidently increased when tumor cells encountered immune cells (Figure 5A), but the increased extent is distinct between MTAP WT and KO cells. Anti-tumoral IL-1α, IL-1β, IL-12 and IFN-γ as well as triggered IP-10, MIP-1α and MIP-1β levels were higher in WT+PBMC, while pro-tumoral IL-6, IL-8 and IL-9 as well as triggered Eotaxin and IL-22 (specific in lung cancer cells) levels were higher in KO+PBMC. CyTOF profiling revealed that despite the difference of each sub-population of immune cells between WT and KO groups was not significant (Figure 5B), the mean intensities of anti-tumoral immune markers Granzyme A, Perforin, CD40L, OX40, GITR, CD278 and CXCR3 were higher in CD45+ cells co-cultured with WT cells, whereas pro-tumoral immune markers CTLA-4, Foxp3 and IL-10 were induced

in CD45+ cells co-cultured with KO cells (Figure 5C).

MTAP deficiency impairs intratumoral immunity to support tumorigenesis

We further systematically analyzed the tumor-infiltrating leukocyte (TIL) population from tumors of humanized mice by CyTOF. In addition to decreased infiltration of immune cells, CyTOF analysis revealed opposite composition of TIL population where T cell, B cell and NK cell sub-populations were less and dendritic cell and monocyte/macrophage sub-populations were more in MTAP-deficient CL1-0 KO and CL1-5 Mock tumors (Figures 6A and 6D). The profiling of immune cell markers (Figures 6B and 6E) also demonstrated that the expression levels of immune cell-expressed pro-tumoral immune markers PD-L1, Arginase 1, CD34, Nectin-2 and CD47 were elevated in CL1-0 MTAP KO tumors compared to CL1-0 WT tumors (Figure 6C), and the intensities of anti-tumoral immune markers CD169, CXCR3 and OX40L were higher in immune cells from CL1-5 MTAP tumors than in the one from CL1-5 Mock tumors (Figure 6F). These results supported that MTAP deficiency in tumors prevents immune cell recruitment and activation, converting tumors to a more immunosuppressive state.

Validation of reshaped immune landscape in MTAP-deficient tumors

Given the convenient accesses to the transcriptomic data of cancer patients from The

Cancer Genome Atlas and to the webtools that can estimate the abundances of cell subsets in a mixed cell population by using gene expression data, the RNA-sequencing data of lung adenocarcinoma (LUAD) and kidney renal clear cell carcinoma (KIRC) cohorts were subjected to the analyses by CIBERSORTx and xCell, and then segregated into high and low MTAP mRNA expression groups, respectively. We noticed that the proportions of B cells naive, T cells CD8 (only in LUAD), T cells CD4 memory resting and activated, T cells gamma delta, NK cells resting and activated (only in LUAD) and Macrophages M1 were lower in low MTAP-expressing tumors, and higher T cells regulatory (Tregs), Monocytes and Dendritic cells resting and activated levels were associated with low MTAP group, as revealed by CIBERSORTx (Figure 7A). In xCell analysis, a similar result was also observed that the subsets of CD4+ memory T cells, CD4+ T cells, CD8+ T cells, NK cells (only in LUAD) and naive B-cells were lesser in low MTAP tumors, while Monocytes (only in LUAD), Macrophages M2 and Dendritic cells (only in LUAD) were more abundant in low MTAP expression group (Figure 7B), supporting our findings in humanized mice (Figures 6A and 6D). In summary, we characterized a new role of MTAP deficiency in the microenvironment that remodels immune profiles and contributes to immune evasion, brightening up a dark corner of oncoimmunology.

DISCUSSION

MTAP, the regulator of polyamine, adenine and methionine metabolic pathways, has been known as a tumor suppressor[17]. Recent studies have further explored the role of MTAP to extend beyond metabolism, suggesting a newfound interaction between proximal cells in the tumor site. Of the different cell populations, immune cells are pioneers to identify and eliminate aberrant neoplastic cells[21]. In this study, we demonstrated that MTAP-deficient tumors intrinsically exhibit altered immune signaling pathways, extrinsically remodel the immune microenvironment, and subsequently escape the immune surveillance, defining a new role of MTAP in immune regulation.

Progress in the field of oncoimmunology can be attributed to suitable animal models, through which comprehensive analyses are accomplished under physiologically-relevant standards. Compared to other murine models such as syngeneic models, humanized mice have more valuable translational prospects due to their inherent [composition], thus sufficing as a robust method to better understand and apply oncoimmune dynamics. Humanized mice have pioneered the forefront of animal studies because of their specificity and stability in generating a compatible system. In addition to being able to support a variety of tumor types, corroborated by high xenograft take

rates and growth rates, these mice harbor human immune systems[22]. Heightened sensitivity and physiological semblance prove to be prominent advantages, making humanized mice attractive pre-clinical models to further investigate immunotherapies. In fact, studies have utilized hu-CB-BRGS and Onco-HuNSG mice to instructively characterize B-cell and T-cell populations in response to PD-L1 treatments[23]. To the best of our knowledge, we are among the first to study tumor immune microenvironment-related consequences of MTAP loss *in vivo* using NSG-SGM3 mice. Consistent with our previous findings, we observed an increase in size of MTAP-loss tumors in immunodeficient mice; similar results were also recapitulated here (Figure 4A). However, we noticed a striking phenomenon in mice that were injected with human hematopoietic stem cells (Figure 4B). While MTAP-expressing tumors have roughly similar sizes with and without immune interaction, the size of MTAP-loss tumors is significantly larger in mice with immune cells, indicating a significant contribution of immunoediting to tumor progression. These results qualitatively depict distinct tumor landscapes between the two groups.

MTAP deletion influences both elements of the tumor and surrounding microenvironment. Our RNA-sequencing data consolidated that signaling pathways related to the immune system were differentially activated in MTAP WT cell lines compared to corresponding

KO cell lines (Figure 1A). We have further highlighted three pathways of interest: CXCR4, IL-5, and IFN-g. These signaling pathways are established in regulating the immune response and indicate that MTAP deletion altered cellular activity at the fundamental level of the transcriptome[24-26]. Cytokines are key chemical messages that regulate the immune system; their role in cancer has predominantly been attributed to influence the surrounding milieu, reshaping tumor composition to mediate [neoplastic] development. Of particular interest, IL-12, IFN-g, and IP-10 were found to be decreased in the MTAP KO group. Predominantly produced by immune cells such as macrophages, dendritic cells, and T cells, these cytokines are crucial to immunity by initiating the adaptive immune response[27]. In fact, IL-12 is necessary to ensure effective PD-1 immunotherapy results; IFN-g released by drug-stimulated T cells induced IL-12 , which resulted in a potent antitumor immune response and tumor reduction[28]. A potential mechanism for this heightened [immunity surge] can be contributed to the IL-12/ IFN-g/ IP-10/ CXCR3 axis. IL-12 is well known to activate IFN-g production, which acts on various cell types to induce IP-10 expression[29]. IP-10 is a chemoattractant for activated lymphocytes and signals through CXCR3, which possess antitumor qualities. Several studies have reported the synergistic effects of IP-10 with chemotherapy and gene therapy, suggesting that this axis has a significant role in reinforcing the efficacy of cancer

treatments[29]. Given that these signaling molecules are implicated in immunity, the apparent reduction upon MTAP deletion may exacerbate tumorigenesis by interfering with the intervening aspects of this process.

Upon further analysis of the cellular composition in the adjacent tumor microenvironment, we noticed significant decreases in total tumor infiltrating lymphocytes (TILs) such as T cells, B cells, NK cells and even M1/ M2 macrophages (Figure 6). Integral to immunosurveillance, these cells are influenced by the amount of neoantigens or cytokines present in the tumor site. T cells are functionally categorized by the type of markers they express; CD4+ T cells prime the immune response by differentiating to specific effector cells upon contact with antigens on MHC class II proteins, whereas CD8+ T cells employ cytotoxic effects through granule exocytosis and Fas ligand (FasL)-dependent apoptosis.23 Members of the CXC and CC family of chemokines are chemotactic for immune cells; in particular, the CXCR3 axis is a major gateway for lymphocyte recruitment. The corresponding ligands (CXCL4, CXCL9, CXCL10, and CXCL11) are induced by IFN-g[30]. Moreover, CXCL13 is implicated in mounting the adaptive immune response; Yang et al. reported that administering CXCL13 led to an increase in CD8+ T cells and CD20+ B cells, thus synergistically augmenting anti-PD-1 therapy[31]. In addition to these lymphocytes, NK cells mediate antitumor immunity and

are recruited to the tumor site by IP-10, CCL21, and CCL27[32].In endometrial cancer, the surrounding microenvironment was characterized by increased IL-6 (a negative regulatory of NK cell activity) and IL-1B, and lower concentrations of several chemoattractants, generating a barren NK cell landscape and dampened cytolytic activity. Similarly, macrophages are recruited to the tumor site by IP-10, CCL2, and CCL5 and polarized into the protumor M2 phenotype[33] [34]. In turn, tumor associated macrophages (TAMs) inhibit CD8+ T cell migration by activating signaling pathways such as the hedgehog pathway, resulting in impaired CXCL9 and IP-10 secretion[35]. Immune infiltrates have been associated with auspicious patient outcomes and the lack thereof due to the immunosuppressive milieu prevents neoplastic cells from being efficiently eliminated. This phenomenon may be responsible for the fact that tumor sizes are more prominent in MTAP KO mice grafted with immune cells compared to immune-deficient mice. Although these mice were injected with hematopoietic stem cells, alteration of the cytokine profile from MTAP loss created an immunologically cold landscape in which there was impaired recruitment and function of immune cells, preventing the incipience and maintenance of an antitumor response.

A successful immune response is instituted in conjunction with antigen presenting cells (APCs), which display MHC class II molecules and antigens on their surfaces. Derived

from hematopoietic stem cells, dendritic cells further differentiate into conventional or non-conventional type subsets, each characterized by residence, morphology, and function[36]. Upon activation, lymphoid DCs travel to the lymph nodes, where they prime CD4+ and CD8+ T cells by secreting IL-12. In cancer, impaired ability of DCs to infiltrate the tumor contributes to an immunosuppressive setting. Although we detected an abundant DC population in MTAP KO mice, the overall immunologically devoid outcome suggests that these DCs may be generated to stimulate lymphocytes but may not be to reach the lymph nodes to actually execute an antitumor response. This paves a future avenue and possibility to study the tumor-immune interplay beyond the context of the immediate tumor microenvironment.

Immune checkpoints are key regulators of the immune system, acting as both positive and negative measures to maintain homeostasis as necessary. The PD-L1/ PD-1 axis is the most well characterized immune checkpoint, notably repressing T cell activity through downstream signaling pathways such as PI3k/Akt. Many cancers including lung, RCC, breast, melanoma, and urothelial exhibit elevated PD-L1 levels, underscoring the prevalence of this phenomenon in tumor progression[37]. In our study we observed a substantial increase in PD-L1 in our MTAP KO cancer cell lines, suggesting that MTAP loss plays a role in upregulating PD-L1 levels. We propose potential mechanisms that

may account for this occurrence. In our previous findings we reported that MTAP deletion mediates crosstalk between epigenetic modifications and tyrosine phosphorylation, particularly IGF1R[17]. Given that MTAP loss stimulates IGF1R yet unaffected PD-L1 mRNA levels, we hypothesize that activation of IGF1R downstream pathways PI3K/Akt may constitute the increase in PD-L1 expression. Impaired protein methylation resulting from MTA-induced PRMT5 inhibition and subsequent loss of symmetric dimethylarginine (sDMA) may also elicit PD-L1 upregulation. Moreover, the altered cytokine composition in the tumor microenvironment may induce PD-L1 expression in cancer cells. In hepatocellular carcinoma, IL-1B secreted from M1 macrophages elicited PD-L1 expression through transcription factors p65 and IRF1[38]. Other pro-inflammatory cytokines such as IL-17 and TNF-a secreted by T helper 17 (TH17) have been shown to prompt PD-L1 translation and thereby aggravate tumor malignancy. Clinically, high PD-L1 levels have been associated with poor response to immunotherapies. Muscle-invasive bladder cancer patients with low expressions of the triad genes MTAP, CDKN2A, and CDKN2B due to a deleted chr9 p21[17]. region were found to have lower response rates to PD-L1 immunotherapy compared to those with an intact chromosome. Given the plausible interaction between MTAP and PD-L1 and its repercussions on cancer progression, it is of great importance to uncover the molecular mechanisms that govern

MTAP loss-induced PD-L1 expression and subsequent T cell exhaustion.

An emerging field in cancer immunology concerning cellular metabolism has garnered much interest in recent decades. A growing array of evidence substantiates the role of intrinsic metabolic pathways in shaping both the immune response and encompassing microenvironment. Key metabolites regulated by MTAP include methionine, adenine, adenosine, SAM, and MTA. Gene expression profiling of prostate cancer tissues identified cysteine, methionine, and nicotinamide adenine dinucleotide metabolism pathways to be differentially activated between normal and malignant groups, thus raising possibilities for new biomarkers. A recent study demonstrated that tumor cells are capable of perturbing methionine metabolism in CD8+ T cells, which repress antitumor immunity via epigenetic alterations and JAK/ STAT5 signaling[39]. Increased extracellular adenosine generated by Tregs has been shown to inhibit the immune response, binding onto A2a receptors on effector T cells to impede their function. Moreover, SAM and its downstream metabolite MTA potentiate suppressive effects on hepatocellular carcinoma-infiltrating T cells; exogenous administration of SAM/MTA resulted in elevated T cell exhaustion transcription factors and diminished T cell activity[40]. Thus, immunometabolism unequivocally emerges as an attractive and crucial prospect to advance [the steamboat of cancer research]. Future research should be directed to

solidify mechanistic understandings of the interchange between the metabolome and immune system and identify molecular targets.

In summary, our results demonstrate that MTAP deletion reconstructs the tumor microenvironment via cytokine reprogramming and restructuring of immune infiltrates thereby promoting cancer malignancy. Our studies shed insight on how metabolic processes contribute to immunologically cold tumors and provide a molecular basis to integrate the multi-faceted nature of cancer to develop efficient therapeutics.

MATERIALS AND METHODS

Reagents and antibodies

RPMI-1640 medium, Dulbecco's modified Eagle's medium (DMEM), fetal bovine serum and penicillin-streptomycin were purchased from Life Technologies (Carlsbad, CA). Red blood cell (RBC) lysis buffer was purchased from Gibco, Thermo Fisher Scientific (Waltham, MA, USA). Nylon mesh for flow cytometry assays was purchased from Becton Dickinson [BD] Falcon (Bedford, MA, USA). Anti-PD-L1 (E1L3N) antibody was purchased from Cell Signaling Technology (Danvers, MA). Anti-MTAP (2G4) antibody was purchased from Abnova (Taipei, Taiwan). Anti-β-actin (GT5512) antibody was purchased from GeneTex (Hsinchu, Taiwan). Goat anti-mouse IgG-HRP and goat anti-rabbit IgG-HRP secondary antibodies were purchased from Santa Cruz Biotechnology (Santa Cruz, CA).

Cell lines and cell culture

786-0 and CL1-0 control (WT) and MTAP-knockout (KO) cells as well as CL1-5 control (Mock) and MTAP-overexpressing (MTAP) cells were established and maintained at 37^{o}C in a humidified atmosphere of 5% CO_2 as previously described[1].

RNA sequencing and pathway analysis

For transcriptome profiling analysis, total RNA was extracted from CL1-5 Mock/MTAP cells, 786-0 WT/KO cells, and CL1-0 WT/KO cells co-cultured with or without PBMCs using TRIzol reagent (Invitrogen), respectively. RNA concentration was determined using the NanoDrop machine (Thermo Fisher Scientific). Complementary DNA (cDNA) was generated using the SuperScript III First Strand cDNA Synthesis Kit (Thermo Fisher Scientific). Transcriptomic profiles were aligned to human genome using Affymetrix gene expression arrays. The RNA sequencing data were deposited in the NCBI SRA database (PRJNA720919). Differential gene expression analysis was performed using the R package DESeq2. Genes with false discovery rate (FDR) < 0.05 and fold change ≧ 2.0 were considered as the significantly differentially expressed genes (DEGs). GSEA was performed using a curated collection of gene sets consisting of sets from the Hallmark and Gene Ontology collections in the MSigDB database[2,3]. MetaCore analytical suite (version 20.4 build 70300) was utilized for pathway analysis on the list of DEGs.

Reverse phase protein array

More than 1×10^6 CL1-0 and 786-0 WT/KO cells were collected and submitted to the RPPA Core Facility, MD Anderson Cancer Center (Houston, TX, USA), for RPPA

analysis. The list of differentially expressed proteins and phosphorylated proteins with $p < 0.05$ were subjected to pathway analysis by using MetaCore analytical suite (version 20.4 build 70300).

Luminex assays

The intracellular concentrations of 35 cytokines/chemokines/growth factors were measured by using the Human Cytokine Magnetic 35-Plex Panel (#LHC6005M, Thermo Fisher Scientific, Waltham, MA) as recommended. Data were acquired using Luminex MAGPIX instrumentation (Luminex Corp., Austin, TX) and analyzed by the xPONENT software package per the manufacturer's protocol. The following molecules were detected: EGF, Eotaxin, FGF basic, G-CSF, GM-CSF, HGF, IFN-α, IFN-γ, IL-1ra, IL-1α, IL-1β, IL-2, IL-2r, IL-3, IL-4, IL-5, IL-6, IL-7, IL-8, IL-9, IL-10, IL-12 (p40/p70), IL-13, IL-15, IL-17A, IL-17F, IL-22, IP-10, MCP-1, MIG, MIP-1α, MIP-1β, RANTES, TNF-α, and VEGF.

Western blot assays

Western blot analyses and the preparations of whole cell lysates have been previously described[1]. Whole cell lysates were prepared with lysis buffer (50 mM Tris-HCl (pH 7.4), 1% NP-40, 150 mM NaCl, 1 mM EDTA, 20 μg/ml leupeptin, 1 mM PMSF and 20 μg/ml

aprotinin), and proteins were then subjected to separating by SDS-PAGE and transferred to polyvinylidene fluoride (PVDF) membranes. Appropriate antibodies were probed on the membranes, followed by enhanced chemiluminescence detection. The images of immunoblotting analysis were quantified by ImageJ software (National Institutes of Health, Bethesda, MD, USA).

Immunofluorescent staining

For cell immunofluorescent staining, 786-0 WT/KO cells cultured on 12 mm glass cover-slips were fixed for 15 minutes in phosphate-buffered saline containing 4% paraformaldehyde and 2% sucrose and then permeabilized in phosphate-buffered saline containing 0.3% Triton X-100 for 2 minutes. Cover-slips were reacted with primary antibody against PD-L1 and Alexa Fluor 594 conjugated anti-rabbit secondary antibody, and nuclei were demarcated with DAPI staining. The cells were mounted onto slides and visualized using the Zeiss LSM510 laser-scanning confocal microscope image system. For tissue immunofluorescent staining, the tissue slides were de-paraffinized, rehydrated, and heated for antigen retrieval. The tissue slides were then reacted with antibodies against Alexa Fluor 594-conjugated CD3-ζ antibody (Santa Cruz Biotechnology, #sc-1239 AF594), Alexa Fluor 488-conjugated NCAM antibody

(Santa Cruz Biotechnology, #sc-7326 AF488), Alexa Fluor 647-conjugated CD19 antibody (Santa Cruz Biotechnology, #sc-19650 AF647), Alexa Fluor 647-conjugated B7-2 antibody (Santa Cruz Biotechnology, #sc-28347 AF647), and/or Alexa Fluor 647-conjugated iNOS antibody (Novus Biologicals, #NBP2-22119AF647) for 1 h at room temperature in the dark. The nuclei were subsequently stained with DAPI. After the slides were mounted in mounting medium, the detection of immunofluorescence was performed using the FluoView FV3000 spectral confocal system (Olympus, Center Valley, PA, USA).

***In vivo* animal experiments**

All mouse experiments and procedures were approved and periodically reviewed by the Institutional Animal Care and Use Committee (IACUC) at UC Davis. Sixteen-week-old male NSG-SGM3 mice (JAX stock #013062) were purchased from the Jackson Laboratory and housed four mice per cage and fed autoclaved food *ad libitum*. For tumorigenicity assay, 1×10^6 cells were suspended in 100 μl PBS and implanted subcutaneously into the dorsal region of mice. Tumor growth was examined twice or thrice a week, and tumor volume was estimated by the formula $LW^2/2$, where L is the length and W is the width of the tumor. After 20 and 27 days, the mice were sacrificed

and the tumor xenografts were removed, weighted, and photographed.

PBMCs or tumor-infiltrating leukocyte profile analysis by CyTOF

For CyTOF analysis, single cells from PBMC co-cultures or tumors prepared by disaggregation of the mixture through a 100-mm nylon mesh were harvested and submitted to the Bioanalytics and Single-Cell (BASiC) Core at UT Health San Antonio (San Antonio, TX, USA)[4]. Briefly, cells were stained with cisplatin- and metal-conjugated surface antibodies sequentially for viability and surface staining. After fixation and permeabilization, cells were stained with metal-conjugated antibodies. The cells were then labeled with an iridium-containing DNA intercalator ($^{191}Ir^{+}$ or $^{193}Ir^{+}$) for identification of cell events before analysis on a Helios mass cytometer. Signals were bead-normalized using EQ Four Element Calibration Beads. Signals of samples were normalized using CyTOF software (Version 6.7.1014, Fluidigm). The generated files underwent signal cleanup and filtering for single cells using Cytobank (https://www.cytobank.org/).

Estimation of infiltrated immune population

The transcriptomic data of LUAD and KIRC patients were extracted from The Cancer Genome Atlas. CIBERSORTx[5] is available as an online tool

(http://cibersortx.stanford.edu). The LM22 immune cell type signature matrix and the setting of 100 for "permutations for significance analysis" were applied for the CIBERSORTx analysis. Cell type analysis of LUAD and KIRC patients using xCell[6] were already available and downloaded from the xCell website (https://xcell.ucsf.edu/).

Statistical analysis

For *in vitro* or *in vivo* studies, the Student *t* test was used to compare the difference between two groups. The difference in patient characteristics between the high-expression and low-expression groups was examined using either Student *t* test or Chi-square test. All statistical analyses were performed using GraphPad Prism software version 7 (GraphPad). All tests were two-tailed, and p values < 0.05 were considered significant.

REFERENCES

1. Robert C, Schachter J, Long GV, et al. Pembrolizumab versus Ipilimumab in Advanced Melanoma. N Engl J Med 2015;372(26):2521-32. doi: 10.1056/NEJMoa1503093

2. Herbst RS, Baas P, Kim DW, et al. Pembrolizumab versus docetaxel for previously treated, PD-L1-positive, advanced non-small-cell lung cancer (KEYNOTE-010): a randomised controlled trial. Lancet 2016;387(10027):1540-50. doi: 10.1016/S0140-6736(15)01281-7

3. Motzer RJ, Escudier B, McDermott DF, et al. Nivolumab versus Everolimus in Advanced Renal-Cell Carcinoma. N Engl J Med 2015;373(19):1803-13. doi: 10.1056/NEJMoa1510665

4. Borcoman E, Kanjanapan Y, Champiat S, et al. Novel patterns of response under immunotherapy. Ann Oncol 2019;30(3):385-96. doi: 10.1093/annonc/mdz003

5. Waldman AD, Fritz JM, Lenardo MJ. A guide to cancer immunotherapy: from T cell basic science to clinical practice. Nat Rev Immunol 2020;20(11):651-68. doi: 10.1038/s41577-020-0306-5

6. Zhao B, Zhao H, Zhao J. Efficacy of PD-1/PD-L1 blockade monotherapy in clinical trials. Ther Adv Med Oncol 2020;12:1758835920937612. doi: 10.1177/1758835920937612

7. Man J, Millican J, Mulvey A, et al. Response Rate and Survival at Key Timepoints With PD-1 Blockade vs Chemotherapy in PD-L1 Subgroups: Meta-Analysis of Metastatic NSCLC Trials. JNCI Cancer Spectrum 2021;5(3) doi: 10.1093/jncics/pkab012

8. Grossman JE, Vasudevan D, Joyce CE, et al. Is PD-L1 a consistent biomarker for anti-PD-1 therapy? The model of balstilimab in a virally-driven tumor. Oncogene 2021;40(8):1393-95. doi: 10.1038/s41388-020-01611-6

9. Robert C, Ribas A, Hamid O, et al. Durable Complete Response After Discontinuation of Pembrolizumab in Patients With Metastatic Melanoma. J Clin Oncol 2018;36(17):1668-74. doi: 10.1200/JCO.2017.75.6270

10. Sharma P, Hu-Lieskovan S, Wargo JA, et al. Primary, Adaptive, and Acquired Resistance to Cancer Immunotherapy. Cell 2017;168(4):707-23. doi: 10.1016/j.cell.2017.01.017

11. Galon J, Bruni D. Approaches to treat immune hot, altered and cold tumours with

combination immunotherapies. Nat Rev Drug Discov 2019;18(3):197-218. doi: 10.1038/s41573-018-0007-y

12. Bonaventura P, Shekarian T, Alcazer V, et al. Cold Tumors: A Therapeutic Challenge for Immunotherapy. Front Immunol 2019;10:168. doi: 10.3389/fimmu.2019.00168

13. Bertino JR, Waud WR, Parker WB, et al. Targeting tumors that lack methylthioadenosine phosphorylase (MTAP) activity: current strategies. Cancer Biol Ther 2011;11(7):627-32. doi: 10.4161/cbt.11.7.14948

14. Kryukov GV, Wilson FH, Ruth JR, et al. MTAP deletion confers enhanced dependency on the PRMT5 arginine methyltransferase in cancer cells. Science 2016;351(6278):1214-8. doi: 10.1126/science.aad5214

15. Marjon K, Cameron MJ, Quang P, et al. MTAP Deletions in Cancer Create Vulnerability to Targeting of the MAT2A/PRMT5/RIOK1 Axis. Cell Rep 2016;15(3):574-87. doi: 10.1016/j.celrep.2016.03.043

16. Mavrakis KJ, McDonald ER, 3rd, Schlabach MR, et al. Disordered methionine metabolism in MTAP/CDKN2A-deleted cancers leads to dependence on PRMT5. Science 2016;351(6278):1208-13. doi: 10.1126/science.aad5944

17. Xu J, Chang WH, Fong LWR, et al. Targeting the insulin-like growth factor-1 receptor in MTAP-deficient renal cell carcinoma. Signal Transduct Target Ther 2019;4:2. doi: 10.1038/s41392-019-0035-z

18. Fahrmann JF, Grapov DD, Wanichthanarak K, et al. Integrated Metabolomics and Proteomics Highlight Altered Nicotinamide- and Polyamine Pathways in Lung Adenocarcinoma. Carcinogenesis 2017;38(3):271-80. doi: 10.1093/carcin/bgw205

19. Fan Z, Kong X, Xia J, et al. The arginine methyltransferase PRMT5 regulates CIITA-dependent MHC II transcription. Biochim Biophys Acta 2016;1859(5):687-96. doi: 10.1016/j.bbagrm.2016.03.004

20. Henrich FC, Singer K, Poller K, et al. Suppressive effects of tumor cell-derived 5'-deoxy-5'-methylthioadenosine on human T cells. Oncoimmunology 2016;5(8):e1184802. doi: 10.1080/2162402X.2016.1184802

21. Jacobs B, Schlogl S, Strobl CD, et al. The Oncometabolite 5'-Deoxy-5'-Methylthioadenosine Blocks Multiple Signaling Pathways of NK Cell Activation. Front Immunol 2020;11:2128. doi: 10.3389/fimmu.2020.02128

22. Morillon YM, Sabzevari A, Schlom J, Greiner JW. The Development of Next-generation PBMC Humanized Mice for Preclinical Investigation of Cancer

Immunotherapeutic Agents. Anticancer Res. 2020 Oct;40(10):5329-5341. doi: 10.21873/anticanres.14540.

23. Capasso A, Lang J, Pitts TM, Jordan KR, Lieu CH, Davis SL, Diamond JR, Kopetz S, Barbee J, Peterson J, Freed BM, Yacob BW, Bagby SM, Messersmith W.A, Slansky JE, Pelanda R, Eckhardt SG. Characterization of immune responses to anti-PD-1 mono and combination immunotherapy in hematopoietic humanized mice implanted with tumor xenografts. Journal for immunotherapy of cancer, 2019 7(1), 37. https://doi.org/10.1186/s40425-019-0518-z

24. Pozzobon T, Goldoni G, Viola A, Molon B. CXCR4 signaling in health and disease. Immunol Lett. 2016 Sep;177:6-15. doi: 10.1016/j.imlet.2016.06.006. Epub 2016 Jun 27. PMID: 27363619.

25. Kandikattu HK, Upparahalli Venkateshaiah S, Mishra A. Synergy of Interleukin (IL)-5 and IL-18 in eosinophil mediated pathogenesis of allergic diseases. Cytokine & growth factor reviews, 2019 47, 83–98. https://doi.org/10.1016/j.cytogfr.2019.05.003

26. Martinez FO, Gordon S, Locati M, & Mantovani A. Transcriptional Profiling of the Human Monocyte-to-Macrophage Differentiation and Polarization: New Molecules and Patterns of Gene Expression. The Journal of Immunology, 2006 177(10), 7303–

7311. https://doi.org/10.4049/jimmunol.177.10.7303

27. Kunze FA, Bauer M, Komuczki J, Lanzinger M, Gunasekera K, Hopp AK, Lehmann M, Becher B, Müller A, Hottiger MO. ARTD1 in Myeloid Cells Controls the IL-12/18–IFN-γ Axis in a Model of Sterile Sepsis, Chronic Bacterial Infection, and Cancer. The Journal of Immunology, 2019 202(5), 1406–1416. https://doi.org/10.4049/jimmunol.1801107

28. Garris CS, Arlauckas SP, Kohler RH, Trefny MP, Garren S, Piot C, Engblom C, Pfirschke C, Siwicki M, Gungabeesoon J, Freeman GJ, Warren SE, Ong S, Browning E, Twitty CG, Pierce RH, Le MH, Algazi AP, Daud AI, Pai SI, Pittet MJ. Successful Anti-PD-1 Cancer Immunotherapy Requires T Cell-Dendritic Cell Crosstalk Involving the Cytokines IFN-γ and IL-12. Immunity, 2018 49(6), 1148–1161.e7. https://doi.org/10.1016/j.immuni.2018.09.024

29. Liu M, Guo S, Stiles JK. The emerging role of CXCL10 in cancer (Review). Oncology letters, 2011 2(4), 583–589. https://doi.org/10.3892/ol.2011.300

30. Cabrero-de Las Heras S, Martínez-Balibrea E. CXC family of chemokines as prognostic or predictive biomarkers and possible drug targets in colorectal cancer. World journal of gastroenterology, 2018 24(42), 4738–4749.

https://doi.org/10.3748/wjg.v24.i42.4738

31. Yang M, Lu J, Zhang G, Wang Y, He M, Xu Q, Xu C, Liu H. CXCL13 shapes immunoactive tumor microenvironment and enhances the efficacy of PD-1 checkpoint blockade in high-grade serous ovarian cancer. Journal for immunotherapy of cancer, 2021 9(1), e001136. https://doi.org/10.1136/jitc-2020-001136

32. Degos C, Heinemann M, Barrou J, Boucherit N, Lambaudie E, Savina A, Gorvel L, Olive D. Endometrial Tumor Microenvironment Alters Human NK Cell Recruitment, and Resident NK Cell Phenotype and Function. Frontiers in immunology, 2019 10, 877. https://doi.org/10.3389/fimmu.2019.00877

33. Chen C, He W, Huang J, Wang B, Li H, Cai Q, Su F, Bi J, Liu H, Zhang B, Jiang N, Zhong G, Zhao Y, Dong W, Lin T. LNMAT1 promotes lymphatic metastasis of bladder cancer via CCL2 dependent macrophage recruitment. Nature communications, 2018 9(1), 3826. https://doi.org/10.1038/s41467-018-06152-x

34. Walens A, DiMarco AV, Lupo R, Kroger BR, Damrauer JS, Alvarez JV. CCL5 promotes breast cancer recurrence through macrophage recruitment in residual tumors. eLife, 2019 8, e43653. https://doi.org/10.7554/eLife.43653

35. Petty AJ, Li A, Wang X, Dai R, Heyman B, Hsu D, Huang X, Yang Y. Hedgehog

signaling promotes tumor-associated macrophage polarization to suppress intratumoral CD8+ T cell recruitment. Journal of Clinical Investigation, 2019 129(12), 5151–5162. https://doi.org/10.1172/jci128644

36. Wang JB, Huang X, Li FR. Impaired dendritic cell functions in lung cancer: a review of recent advances and future perspectives. Cancer Commun 2019 39, 43. https://doi.org/10.1186/s40880-019-0387-3

37. Dermani FK, Samadi P, Rahmani G, Kohlan AK, Najafi R. PD-1/PD-L1 immune checkpoint: Potential target for cancer therapy. Journal of Cellular Physiology. 2018 doi:10.1002/jcp.27172

38. Zong Z, Zou J, Mao R, Ma C, Li N, Wang J, Wang X, Zhou H, Zhang L, Shi Y. M1 Macrophages Induce PD-L1 Expression in Hepatocellular Carcinoma Cells Through IL-1β Signaling. Frontiers in immunology, 2019 10, 1643. https://doi.org/10.3389/fimmu.2019.01643

39. Bian Y, Li W, Kremer DM, Sajjakulnukit P, Li S, Crespo J, Nwosu ZC, Zhang L, Czerwonka A, Pawłowska A, Xia H, Li J, Liao P, Yu J, Vatan L, Szeliga W, Wei S, Grove S, Liu JR, McLean K, Zou W. Cancer SLC43A2 alters T cell methionine metabolism and histone methylation. Nature, 2020 585(7824), 277–282.

https://doi.org/10.1038/s41586-020-2682-1

40. Hung MH, Lee JS, Ma C. Diggs LP, Heinrich S, Chang CW, Ma L, Forgues M, Budhu A, Chaisaingmongkol J, Ruchirawat m, Ruppin E, Greten TF, Wang XW. Tumor methionine metabolism drives T-cell exhaustion in hepatocellular carcinoma. Nat Commun 2020 12, 1455. https://doi.org/10.1038/s41467-021-21804-1

LEGEND

Figure 1. MTAP plays a role in tumor-intrinsic immune signalings.

(**A**) Gene Set Enrichment Analyses (GSEA) of transcriptomic data from CL1-5 Mock/MTAP-overexpressing (MTAP), CL1-0 WT/MTAP KO (KO) and 786-0 WT/MTAP KO (KO) cells were performed using the HALLMARK gene sets. (**B**) MTAP-altered immune-related pathways in CL1-0 cells were identified by the MetaCore analytical suite (version 20.4 build 70300). The differentially expressed genes involved in these pathways were displayed by heatmap graph (right). (**C**) Top 10 ranking pathways of CL1-0 and 786-0 WT/KO cells were enriched by differentially expressed proteins measured by Reverse Phase Protein Array (RPPA). Orange bars: immune-related pathways. (**D**) The signaling direction of the immune-related pathway network objects derived from both RPPA results of CL1-0 and 786-0.

Figure 2. GSEA enrichment for MTAP functions.

(**A**-**C**) GSEA for gene signatures of immune-related hallmarks in CL1-5 Mock/MTAP (**A**), CL1-0 WT/KO (**B**) and 786-0 WT/KO (**C**).

Figure 3. MTAP deficiency enhances tumor immunosuppressive effect.

(**A**) Analysis of cytokines secreted from CL1-0 and 786-0 WT/KO cells by Luminex Multiplex Assays. The semiquantitative results of cytokine secretion levels were represented as heatmap graphs (n=3). (**B**) Western blot analysis of cellular PD-L1 expression levels in CL1-0 and 786-0 WT/KO cells. The number indicates the quantification of three independent Western blots. (**C**) Representative immunofluorescent images of cellular PD-L1 expression levels in 786-0 WT/KO cells. (**D**) Flow cytometric analysis comparing cell surface PD-L1 levels between 786-0 WT/KO cells. The mean fluorescence intensity (MFI) of each cell population was quantified by FlowJo. Isotype: isotype negative control. (**E**) The viability of CL1-0 and 786-0 WT/KO cells after co-cultured with PBMCs for 48 h. Data are presented as mean ± SD (n=3). *$p < 0.05$.

Figure 4. MTAP deficiency promotes tumorigenesis and immune dysfunction.

(**A**) Tumor growth of subcutaneously injected CL1-0 WT/KO and CL1-5 Mock/MTAP cells in NSG-SGM3 humanized mice was measured every three days and dissected at Day 27 (four mice per group). (**B**) Tumor growth of subcutaneously injected CL1-0 WT/KO and CL1-5 Mock/MTAP cells in NSG-SGM3 humanized mice engrafted with human hematopoietic stem cells was measured every two days and dissected at Day 20 (four mice per group). (**C**) The differentially expressed genes (DEGs) with ≧2-fold change from

the comparison of WT cells/WT cells co-cultured with PBMCs (WT/WT+PBMC, 749 genes) and KO cells/KO cells co-cultured with PBMCs (KO/KO+PBMC, 704 genes) were intersected and presented as Venn diagram. 279 genes altered only in WT cells and 234 genes altered only in KO cells were subjected to pathway analysis by the MetaCore analytical suite respectively. (**D**) Top 20 ranking pathways enriched by the 279 genes (orange bars) and 234 genes (purple bars) from (**C**). The pathway order was ranked by the -log(pValue) of orange bars. (**E**) GSEA of the gene set GO_RESPONSE_TO_INTERFERON_GAMMA between WT cells co-cultured with PBMCs (WT+PBMC) and KO cells co-cultured with PBMCs (KO+PBMC). NES: normalized enrichment score. FDR: false discovery rate.

Figure 5. Immune cell responses were reshaped by MTAP-deficient tumor cells.

(**A**) Secreted cytokine levels of CL1-0 and 786-0 WT/KO cells co-cultured with or without PBMCs were determined by Luminex Multiplex Assays. The semiquantitative results of cytokine secretion levels were represented as heatmap graphs. PBMCs were isolated from three different donors. (**B**) Main sub-populations of CD45+ PBMCs co-cultured with CL1-0 WT/KO cells from CyTOF analysis were shown as t-distributed stochastic neighbor embedding (t-SNE) plots. (**C**) t-SNE plots displaying the expression levels of immune cell

markers in CD45+ PBMCs co-cultured with CL1-0 WT/KO cells. Bottom bars: the relative intensities of markers in CD45+ PBMCs co-cultured with CL1-0 WT (blue) or KO (red) cells.

Figure 6. Impaired intratumoral immunity enhances MTAP-deficient tumor growth.

(**A**,**D**) Percentage of immune cell populations within CD45+ TILs from CL1-0 WT/KO (**A**) and CL1-5 Mock/MTAP (**D**) tumors of humanized mice was assessed by CyTOF analysis (four mice per group). (**B**,**E**) Main sub-populations of CD45+ TILs from CL1-0 WT/KO (**B**) and CL1-5 Mock/MTAP (**E**) tumors of humanized mice derived from CyTOF analysis were shown as t-SNE plots. (**C**,**F**) t-SNE plots displaying the expression levels of immune cell markers in CD45+ TILs from CL1-0 WT/KO (**C**) and CL1-5 Mock/MTAP (**F**) tumors of humanized mice. Bottom bars: the relative intensities of markers in CD45+ TILs from CL1-0 WT (blue) and KO (red) tumors, or CL1-5 Mock (red) and MTAP (blue) tumors.

Figure 7. Comparison of immune cell populations between MTAP-expressing and MTAP-deficient tumors.

(**A**,**B**) Estimated proportion of immune subpopulations in lung adenocarcinoma (LUAD) and kidney renal clear cell carcinoma (KIRC) patients with high or low MTAP mRNA expression from The Cancer Genome Atlas Program was analyzed by computational

deconvolution of transcriptomics data using Cibersort (**B**) and xCell (**C**). *$p < 0.05$.

FIGURES

Figure 1

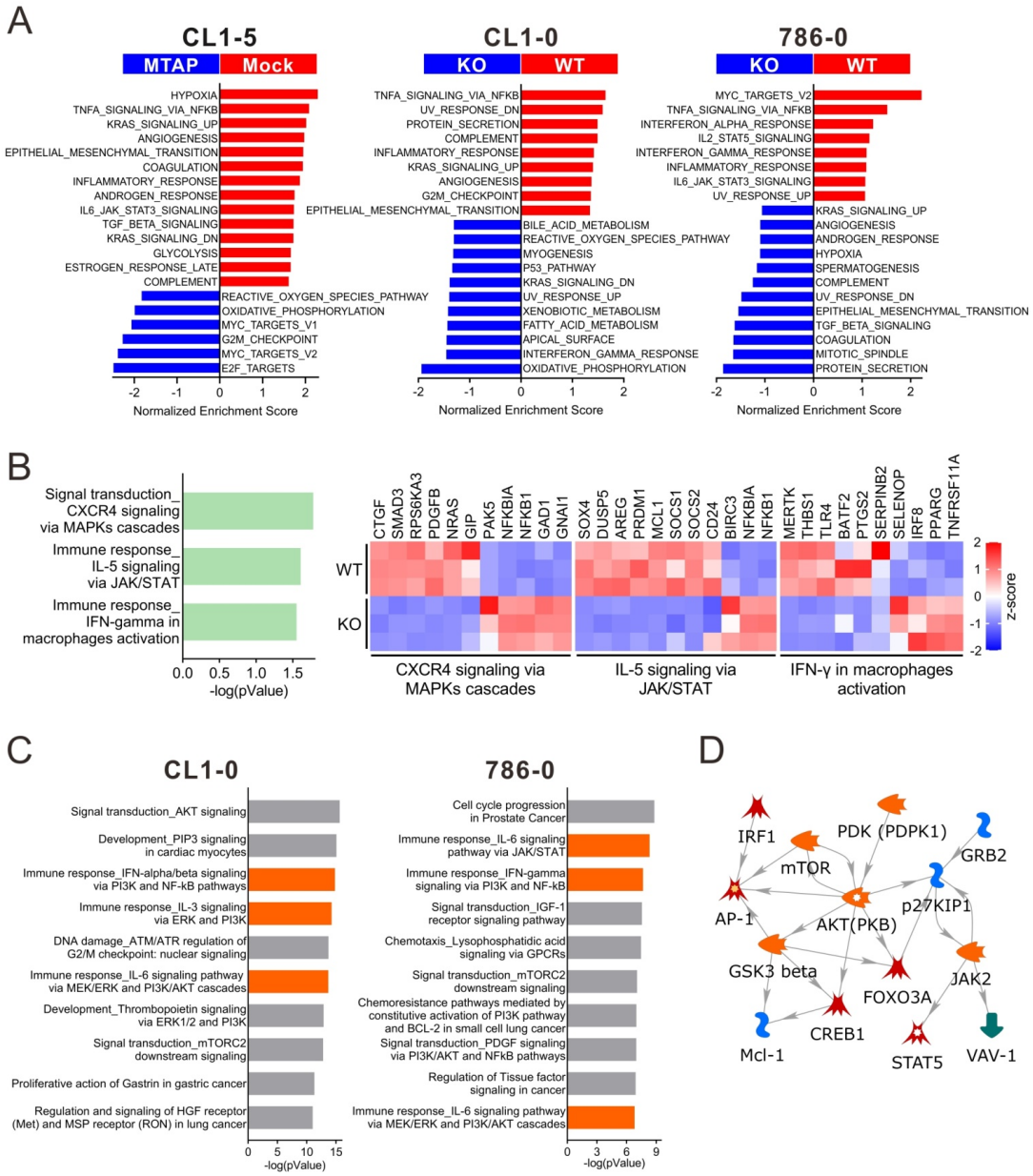

Figure 2

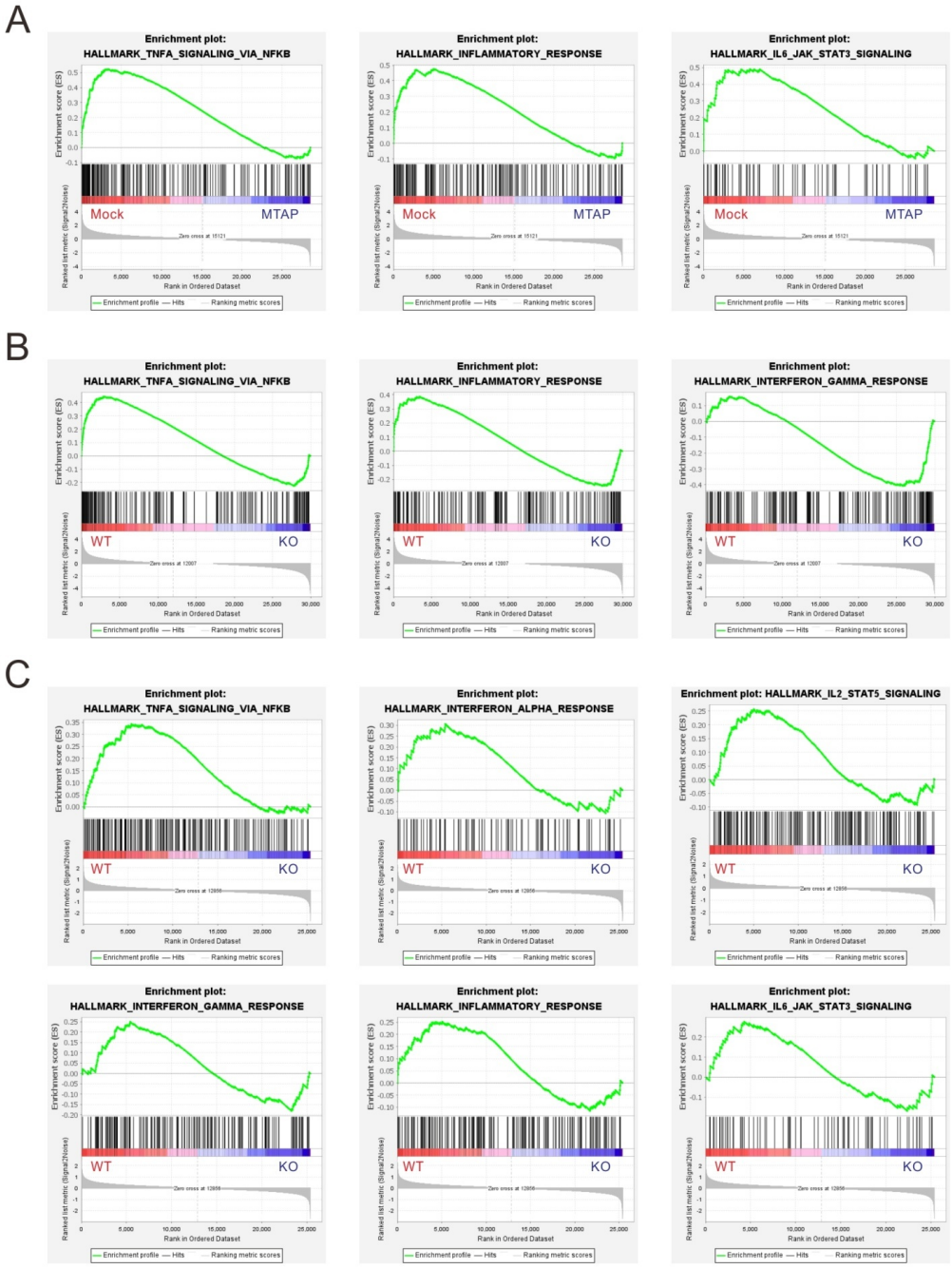
A
Enrichment plot:
HALLMARK_TNFA_SIGNALING_VIA_NFKB
Enrichment plot:
HALLMARK_INFLAMMATORY_RESPONSE
Enrichment plot:
HALLMARK_IL6_JAK_STAT3_SIGNALING
Mock
MTAP
B
Enrichment plot:
HALLMARK_TNFA_SIGNALING_VIA_NFKB
Enrichment plot:
HALLMARK_INFLAMMATORY_RESPONSE
Enrichment plot:
HALLMARK_INTERFERON_GAMMA_RESPONSE
WT
KO
C
Enrichment plot:
HALLMARK_TNFA_SIGNALING_VIA_NFKB
Enrichment plot:
HALLMARK_INTERFERON_ALPHA_RESPONSE
Enrichment plot: HALLMARK_IL2_STAT5_SIGNALING
Enrichment plot:
HALLMARK_INTERFERON_GAMMA_RESPONSE
Enrichment plot:
HALLMARK_INFLAMMATORY_RESPONSE
Enrichment plot:
HALLMARK_IL6_JAK_STAT3_SIGNALING
WT
KO
Enrichment score (ES)
Ranked list metric (Signal2Noise)
Rank in Ordered Dataset
Enrichment profile
Hits
Ranking metric scores

Figure 3

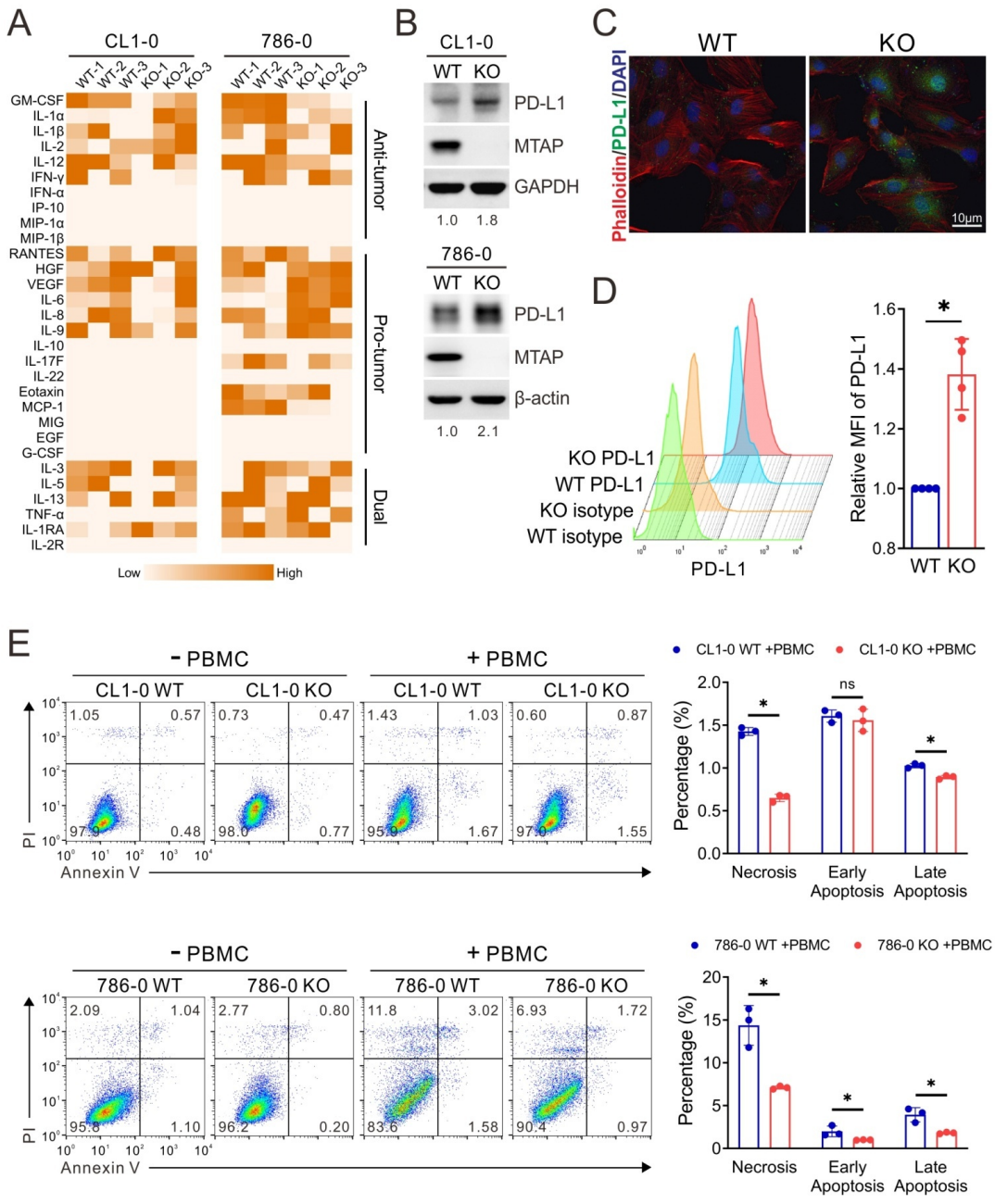
A
CL1-0
786-0
WT-1
WT-2
WT-3
KO-1
KO-2
KO-3
GM-CSF
IL-1α
IL-1β
IL-2
IL-12
IFN-γ
IFN-α
IP-10
MIP-1α
MIP-1β
RANTES
HGF
VEGF
IL-6
IL-8
IL-9
IL-10
IL-17F
IL-22
Eotaxin
MCP-1
MIG
EGF
G-CSF
IL-3
IL-5
IL-13
TNF-α
IL-1RA
IL-2R
Anti-tumor
Pro-tumor
Dual
Low
High
B
CL1-0
WT
KO
PD-L1
MTAP
GAPDH
1.0
1.8
786-0
WT
KO
PD-L1
MTAP
β-actin
1.0
2.1
C
WT
KO
Phalloidin/PD-L1/DAPI
10μm
D
KO PD-L1
WT PD-L1
KO isotype
WT isotype
PD-L1
Relative MFI of PD-L1
1.6
1.4
1.2
1.0
0.8
*
WT
KO
E
- PBMC
+ PBMC
CL1-0 WT
CL1-0 KO
CL1-0 WT
CL1-0 KO
1.05
0.57
0.73
0.47
1.43
1.03
0.60
0.87
97.9
0.48
98.0
0.77
95.0
1.67
97.0
1.55
PI
Annexin V
CL1-0 WT +PBMC
CL1-0 KO +PBMC
Percentage (%)
2.0
1.5
1.0
0.5
0.0
*
ns
*
Necrosis
Early Apoptosis
Late Apoptosis
- PBMC
+ PBMC
786-0 WT
786-0 KO
786-0 WT
786-0 KO
2.09
1.04
2.77
0.80
11.8
3.02
6.93
1.72
95.8
1.10
96.2
0.20
83.6
1.58
90.4
0.97
PI
Annexin V
786-0 WT +PBMC
786-0 KO +PBMC
Percentage (%)
20
15
10
5
0
*
*
*
Necrosis
Early Apoptosis
Late Apoptosis

Figure 4

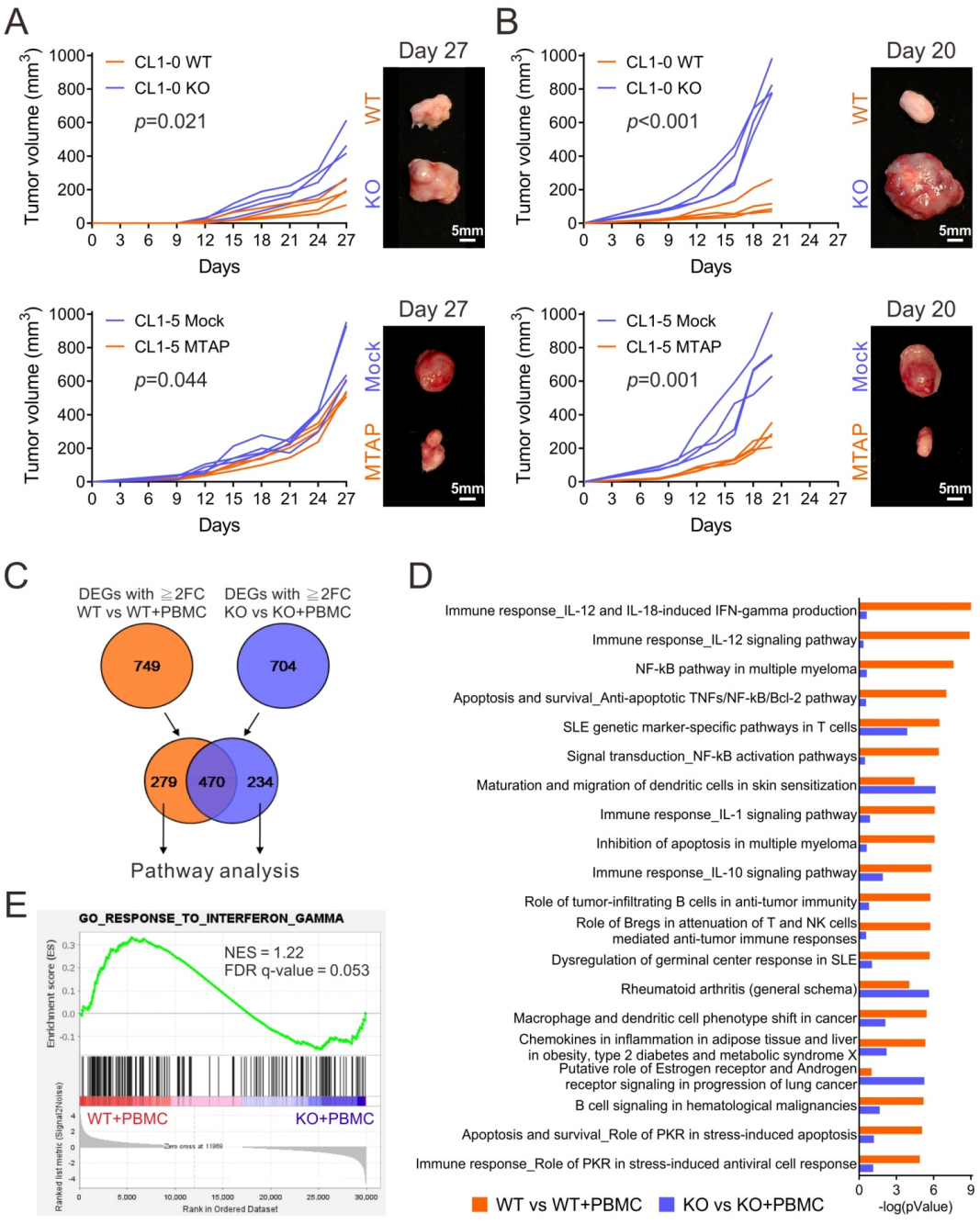
A
B
Tumor volume (mm3)
CL1-0 WT
CL1-0 KO
p=0.021
p<0.001
Day 27
Day 20
WT
KO
5mm
Days
CL1-5 Mock
CL1-5 MTAP
p=0.044
p=0.001
Mock
MTAP
C
DEGs with ≧2FC
WT vs WT+PBMC
DEGs with ≧2FC
KO vs KO+PBMC
749
704
279
470
234
Pathway analysis
D
Immune response_IL-12 and IL-18-induced IFN-gamma production
Immune response_IL-12 signaling pathway
NF-kB pathway in multiple myeloma
Apoptosis and survival_Anti-apoptotic TNFs/NF-kB/Bcl-2 pathway
SLE genetic marker-specific pathways in T cells
Signal transduction_NF-kB activation pathways
Maturation and migration of dendritic cells in skin sensitization
Immune response_IL-1 signaling pathway
Inhibition of apoptosis in multiple myeloma
Immune response_IL-10 signaling pathway
Role of tumor-infiltrating B cells in anti-tumor immunity
Role of Bregs in attenuation of T and NK cells mediated anti-tumor immune responses
Dysregulation of germinal center response in SLE
Rheumatoid arthritis (general schema)
Macrophage and dendritic cell phenotype shift in cancer
Chemokines in inflammation in adipose tissue and liver in obesity, type 2 diabetes and metabolic syndrome X
Putative role of Estrogen receptor and Androgen receptor signaling in progression of lung cancer
B cell signaling in hematological malignancies
Apoptosis and survival_Role of PKR in stress-induced apoptosis
Immune response_Role of PKR in stress-induced antiviral cell response
WT vs WT+PBMC
KO vs KO+PBMC
-log(pValue)
E
GO_RESPONSE_TO_INTERFERON_GAMMA
NES = 1.22
FDR q-value = 0.053
Enrichment score (ES)
WT+PBMC
KO+PBMC
Ranked list metric (Signal2Noise)
Rank in Ordered Dataset

Figure 5

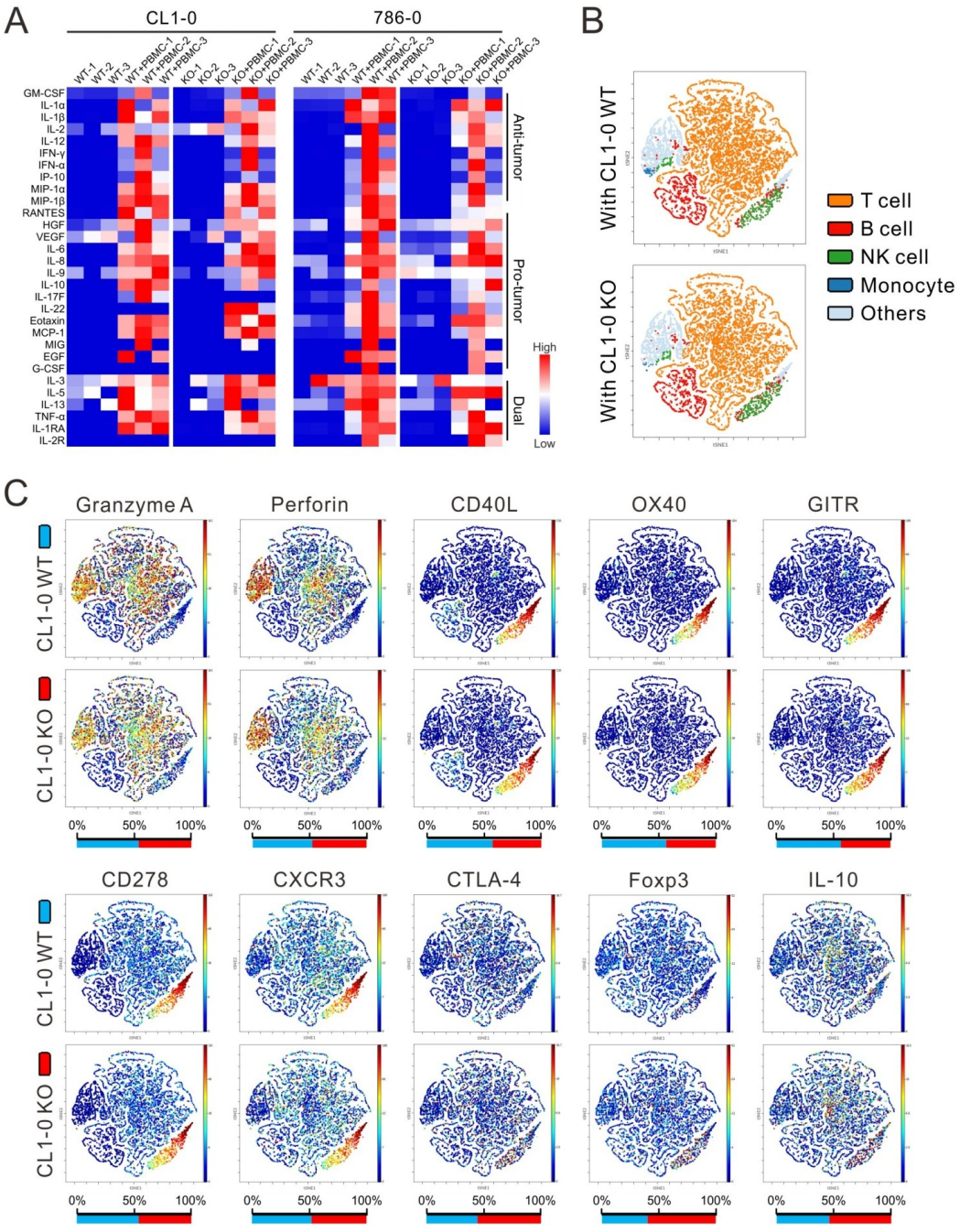
A
CL1-0
786-0
WT-1
WT-2
WT-3
WT+PBMC-1
WT+PBMC-2
WT+PBMC-3
KO-1
KO-2
KO-3
KO+PBMC-1
KO+PBMC-2
KO+PBMC-3
GM-CSF
IL-1α
IL-1β
IL-2
IL-12
IFN-γ
IFN-α
IP-10
MIP-1α
MIP-1β
RANTES
HGF
VEGF
IL-6
IL-8
IL-9
IL-10
IL-17F
IL-22
Eotaxin
MCP-1
MIG
EGF
G-CSF
IL-3
IL-5
IL-13
TNF-α
IL-1RA
IL-2R
Anti-tumor
Pro-tumor
Dual
High
Low
B
With CL1-0 WT
With CL1-0 KO
T cell
B cell
NK cell
Monocyte
Others
C
Granzyme A
Perforin
CD40L
OX40
GITR
CL1-0 WT
CL1-0 KO
0%
50%
100%
CD278
CXCR3
CTLA-4
Foxp3
IL-10

Figure 6

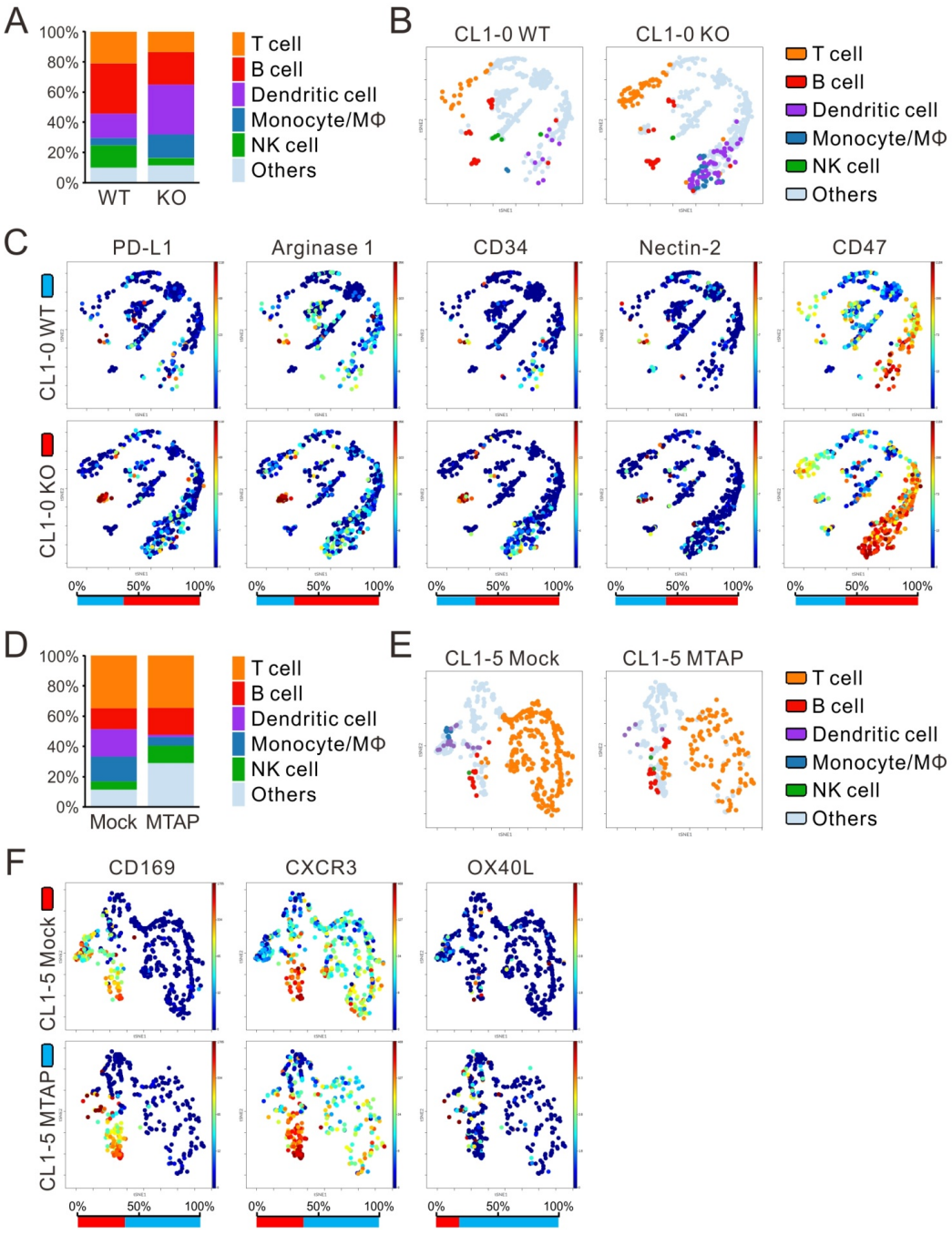
A
100%
80%
60%
40%
20%
0%
WT
KO
T cell
B cell
Dendritic cell
Monocyte/MΦ
NK cell
Others
B
CL1-0 WT
CL1-0 KO
T cell
B cell
Dendritic cell
Monocyte/MΦ
NK cell
Others
C
PD-L1
Arginase 1
CD34
Nectin-2
CD47
CL1-0 WT
CL1-0 KO
0%
50%
100%
D
100%
80%
60%
40%
20%
0%
Mock
MTAP
T cell
B cell
Dendritic cell
Monocyte/MΦ
NK cell
Others
E
CL1-5 Mock
CL1-5 MTAP
T cell
B cell
Dendritic cell
Monocyte/MΦ
NK cell
Others
F
CD169
CXCR3
OX40L
CL1-5 Mock
CL1-5 MTAP
0%
50%
100%

Figure 7

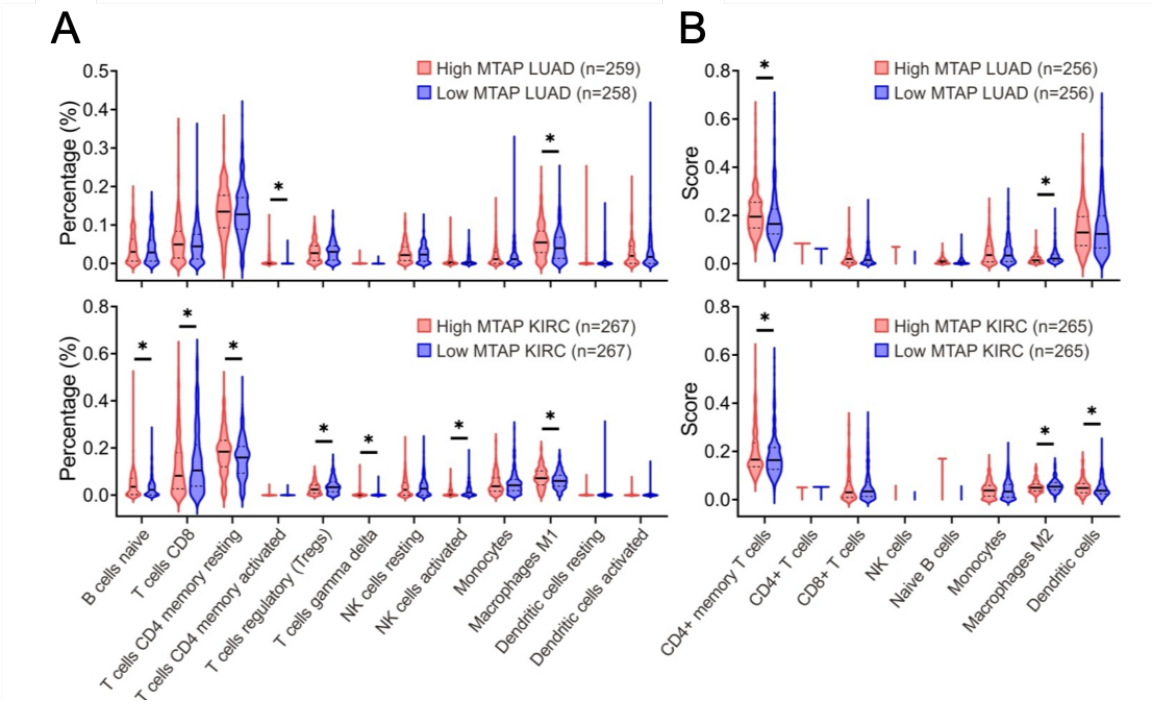
A
High MTAP LUAD (n=259)
Low MTAP LUAD (n=258)
Percentage (%)
High MTAP KIRC (n=267)
Low MTAP KIRC (n=267)
Percentage (%)
B cells naive
T cells CD8
T cells CD4 memory resting
T cells CD4 memory activated
T cells regulatory (Tregs)
T cells gamma delta
NK cells resting
NK cells activated
Monocytes
Macrophages M1
Dendritic cells resting
Dendritic cells activated
B
High MTAP LUAD (n=256)
Low MTAP LUAD (n=256)
Score
High MTAP KIRC (n=265)
Low MTAP KIRC (n=265)
Score
CD4+ memory T cells
CD4+ T cells
CD8+ T cells
NK cells
Naive B cells
Monocytes
Macrophages M2
Dendritic cells